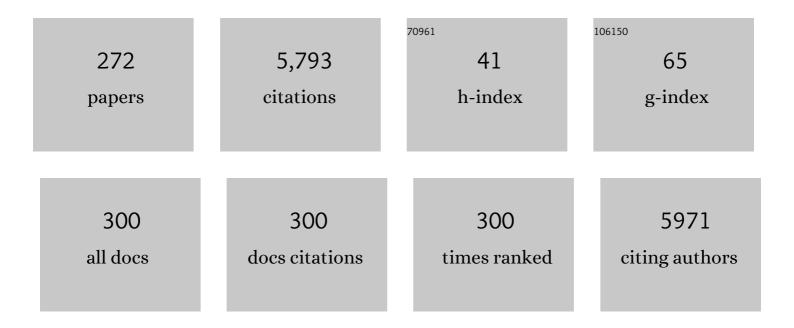
List of Publications by Year in descending order

Source: https://exaly.com/author-pdf/9134046/publications.pdf Version: 2024-02-01



#	Article	IF	CITATIONS
1	Virtual histology of an entire mouse brain from formalin fixation to paraffin embedding. Part 2: Volumetric strain fields and local contrast changes. Journal of Neuroscience Methods, 2022, 365, 109385.	1.3	11
2	Comparative hard x-ray tomography for virtual histology of zebrafish larva, human tooth cementum, and porcine nerve. Journal of Medical Imaging, 2022, 9, 031507.	0.8	7
3	Three-dimensional imaging and analysis of annual layers in tree trunk and tooth cementum. , 2022, , .		0
4	Combining High-Resolution Hard X-ray Tomography and Histology for Stem Cell-Mediated Distraction Osteogenesis. Applied Sciences (Switzerland), 2022, 12, 6286.	1.3	2
5	Three-dimensional analysis of aligner gaps and thickness distributions, using hard x-ray tomography with micrometer resolution. Journal of Medical Imaging, 2022, 9, .	0.8	5
6	Accuracy of commercial intraoral scanners. Journal of Medical Imaging, 2021, 8, 035501.	0.8	6
7	Hard X-ray microtomography of Zebrafish larvae. , 2021, , .		1
8	Historic beaten-copper cranium. , 2021, , .		0
9	Extended-field synchrotron microtomography for non-destructive analysis of incremental lines in archeological human teeth cementum. , 2021, , .		3
10	Mechanistic Illustration: How Newly-Formed Blood Vessels Stopped by the Mineral Blocks of Bone Substitutes Can Be Avoided by Using Innovative Combined Therapeutics. Biomedicines, 2021, 9, 952.	1.4	5
11	Impact of fixation and paraffin embedding on mouse brain morphology: a synchrotron radiation-based tomography study. , 2021, , .		3
12	Virtual histology of an entire mouse brain from formalin fixation to paraffin embedding. Part 1: Data acquisition, anatomical feature segmentation, tracking global volume and density changes. Journal of Neuroscience Methods, 2021, 364, 109354.	1.3	20
13	Reentry of endodontic access cavities: composite residue and loss of tooth substance. Swiss Dental Journal, 2021, 131, .	0.4	0
14	Scavenging of Dickkopf-1 by macromer-based biomaterials covalently decorated with sulfated hyaluronan displays pro-osteogenic effects. Acta Biomaterialia, 2020, 114, 76-89.	4.1	15
15	Hierarchically structured polydimethylsiloxane films for ultra-soft neural interfaces. Micro and Nano Engineering, 2020, 7, 100051.	1.4	6
16	Allometric and Phylogenetic Aspects of Stapes Morphology in Ruminantia (Mammalia, Artiodactyla). Frontiers in Earth Science, 2020, 8, .	0.8	7
17	Shedding Light on Metalâ€Based Nanoparticles in Zebrafish by Computed Tomography with Micrometer Resolution. Small, 2020, 16, e2000746.	5.2	11
18	Simultaneous Three-Dimensional Vascular and Tubular Imaging of Whole Mouse Kidneys With X-ray μCT. Microscopy and Microanalysis, 2020, 26, 731-740.	0.2	7

#	Article	IF	CITATIONS
19	Optimizing contrast and spatial resolution in hard x-ray tomography of medically relevant tissues. Applied Physics Letters, 2020, 116, .	1.5	10
20	Crosslinkable polymeric contrast agent for high-resolution X-ray imaging of the vascular system. Chemical Communications, 2020, 56, 5885-5888.	2.2	9
21	Small-Angle Neutron Scattering Study of Temperature-Induced Structural Changes in Liposomes. Langmuir, 2019, 35, 11210-11216.	1.6	6
22	Spatially resolved small-angle X-ray scattering for characterizing mechanoresponsive liposomes using microfluidics. Materials Today Bio, 2019, 1, 100003.	2.6	10
23	Ex vivo evaluation of an atherosclerotic human coronary artery via histology and high-resolution hard X-ray tomography. Scientific Reports, 2019, 9, 14348.	1.6	6
24	Sensitivity comparison of absorption and grating-based phase tomography of paraffin-embedded human brain tissue. Applied Physics Letters, 2019, 114, .	1.5	12
25	PDE10A mutation in two sisters with a hyperkinetic movement disorder - Response to levodopa. Parkinsonism and Related Disorders, 2019, 63, 240-242.	1.1	5
26	Toward genome editing in X-linked RP—development of a mouse model with specific treatment relevant features. Translational Research, 2019, 203, 57-72.	2.2	6
27	Recent trends in high-resolution hard x-ray tomography. , 2019, , .		3
28	Observations on the scaling relationship between bony labyrinth, skull size and body mass in ruminants. , 2019, , .		7
29	Imaging the internal structure of Borelis schlumbergeri Reichel (1937): Advances by high-resolution hard X-ray microtomography. Palaeontologia Electronica, 2019, 22, .	0.9	4
30	Zugangsrealitäzu S3 Leitlinien gerechten Adipositasoperationen in Deutschland. Zeitschrift Fur Gastroenterologie, 2019, 57, .	0.2	0
31	Evaluation of metal nanoparticle- and plastic resin-based x-ray contrast agents for kidney capillary imaging. , 2019, , .		2
32	Three-dimensional characterization of soft silicone elements for intraoral device. , 2019, , .		1
33	Comparing the accuracy of intraoral scanners, using advanced micro computed tomography. , 2019, , .		3
34	Correction of phase wrapping artifacts in grating-based hard x-ray tomography. , 2019, , .		0
35	Cone-beam computed tomography - magnetic resonance imaging registration in dento-maxillary imaging. , 2019, , .		Ο
36	Polydimethylsiloxane films engineered for smart nanostructures. Microelectronic Engineering, 2018, 194, 1-7.	1.1	4

#	Article	IF	CITATIONS
37	Implementation of a double-grating interferometer for phase-contrast computed tomography in a conventional system nanotom® m. APL Bioengineering, 2018, 2, 016106.	3.3	13
38	Automatic deformable registration of histological slides to $^{1}\!4$ CT volume data. Journal of Microscopy, 2018, 271, 49-61.	0.8	8
39	Three-dimensional imaging and analysis of entire peripheral nerves after repair and reconstruction. Journal of Neuroscience Methods, 2018, 295, 37-44.	1.3	11
40	Three-dimensional and non-destructive characterization of nerves inside conduits using laboratory-based micro computed tomography. Journal of Neuroscience Methods, 2018, 294, 59-66.	1.3	10
41	Propagation-based X-ray Phase Contrast Microtomography of Zebrafish Embryos to Understand Drug Delivery. Microscopy and Microanalysis, 2018, 24, 406-407.	0.2	0
42	Hard X-ray Nano-Holotomography of Formalin-Fixated and Paraffin-Embedded Human Brain Tissue. Microscopy and Microanalysis, 2018, 24, 354-355.	0.2	5
43	Double Grating Interferometry in a Commercial Micro Computed Tomography System for Biomedical Imaging. Microscopy and Microanalysis, 2018, 24, 388-389.	0.2	0
44	A quantitative correction for phase wrapping artifacts in hard X-ray grating interferometry. Applied Physics Letters, 2018, 113, .	1.5	7
45	1. Nanomedicine at a glance. , 2018, , 3-15.		0
46	The bony labyrinth of toothed whales reflects both phylogeny and habitat preferences. Scientific Reports, 2018, 8, 7841.	1.6	29
47	Volumetric Nanoscale Imaging: Hard X-Ray Nanoholotomography: Large-Scale, Label-Free, 3D Neuroimaging beyond Optical Limit (Adv. Sci. 6/2018). Advanced Science, 2018, 5, 1870036.	5.6	0
48	Automated Analysis of Spatially Resolved X-ray Scattering and Micro Computed Tomography of Artificial and Natural Enamel Carious Lesions. Journal of Imaging, 2018, 4, 81.	1.7	6
49	Visualization and Segmentation of Cells in Unstained Paraffin-Embedded Cerebral Tissue. Microscopy and Microanalysis, 2018, 24, 408-409.	0.2	1
50	Hard Xâ€Ray Nanoholotomography: Large‣cale, Labelâ€Free, 3D Neuroimaging beyond Optical Limit. Advanced Science, 2018, 5, 1700694.	5.6	45
51	Conducting and stretchable nanometer-thin gold/thiol-functionalized polydimethylsiloxane films. Journal of Nanophotonics, 2018, 12, 1.	0.4	5
52	Immunocompatibility of Rad-PC-Rad liposomes in vitro, based on human complement activation and cytokine release. Precision Nanomedicine, 2018, 1, 43-62.	0.4	4
53	Highly compliant nanometer-thin Au electrodes exploiting the binding to thiol-functionalized polydimethylsiloxane films. , 2018, , .		0
54	Special Section Guest Editorial: Nanoscience and Biomaterials in Photonics. Journal of Nanophotonics, 2018, 12, 1.	0.4	0

Bert MÃ1⁄4ller

#	Article	IF	CITATIONS
55	Single and double grating-based X-ray microtomography using synchrotron radiation. Applied Physics Letters, 2017, 110, .	1.5	12
56	Liposomes: bio-inspired nano-containers for physically triggered targeted drug delivery. , 2017, , .		2
57	Leakage current, self-clearing and actuation efficiency of nanometer-thin, low-voltage dielectric elastomer transducers tailored by thermal evaporation. Proceedings of SPIE, 2017, , .	0.8	4
58	Electrospraying and ultraviolet light curing of nanometer-thin polydimethylsiloxane membranes for low-voltage dielectric elastomer transducers. , 2017, , .		2
59	Timeâ€Resolved Plasmonics used to On‣ine Monitor Metal/Elastomer Deposition for Lowâ€Voltage Dielectric Elastomer Transducers. Advanced Electronic Materials, 2017, 3, 1700073.	2.6	6
60	Biomimetic nanostructures for the silicone-biosystem interface: tuning oxygen-plasma treatments of polydimethylsiloxane. European Journal of Nanomedicine, 2017, 9, .	0.6	4
61	Biomimetic Remineralization of Carious Lesions by Self-Assembling Peptide. Journal of Dental Research, 2017, 96, 790-797.	2.5	103
62	Nanomechanical probing of thin-film dielectric elastomer transducers. Applied Physics Letters, 2017, 111, .	1.5	7
63	Bony labyrinth morphology clarifies the origin and evolution of deer. Scientific Reports, 2017, 7, 13176.	1.6	45
64	Gold Layers on Elastomers near the Critical Stress Regime. Advanced Materials Technologies, 2017, 2, 1700105.	3.0	16
65	Immunological response to nitroglycerin-loaded shear-responsive liposomes in vitro and in vivo. Journal of Controlled Release, 2017, 264, 14-23.	4.8	15
66	Nanostructure Formation: Timeâ€Resolved Plasmonics used to Onâ€Line Monitor Metal/Elastomer Deposition for Lowâ€Voltage Dielectric Elastomer Transducers (Adv. Electron. Mater. 8/2017). Advanced Electronic Materials, 2017, 3, .	2.6	0
67	Prenatal growth stages show the development of the ruminant bony labyrinth and petrosal bone. Journal of Anatomy, 2017, 230, 347-353.	0.9	33
68	Hard X-ray submicrometer tomography of human brain tissue at Diamond Light Source. Journal of Physics: Conference Series, 2017, 849, 012030.	0.3	1
69	Multimodal imaging of the human knee down to the cellular level. Journal of Physics: Conference Series, 2017, 849, 012026.	0.3	5
70	X-ray micro computed tomography for the visualization of an atherosclerotic human coronary artery. Journal of Physics: Conference Series, 2017, 849, 012002.	0.3	0
71	Grating-based tomography applications in biomedical engineering. , 2017, , .		1
72	Removing ring artefacts from synchrotron radiation-based hard x-ray tomography data. , 2017, , .		0

5

#	Article	IF	CITATIONS
73	Recent trends in high-resolution x-ray tomography. , 2017, , .		1
74	Imaging cellular and subcellular structure of human brain tissue using micro computed tomography. , 2017, , .		0
75	Innervation of the cowâ \in ${}^{\mathrm{M}}$ s inner ear derived from micro-computed tomography. , 2017, , .		1
76	X-ray microscopy of soft and hard human tissues. AIP Conference Proceedings, 2016, , .	0.3	1
77	Electrospraying Nanometerâ€Thin Elastomer Films for Lowâ€Voltage Dielectric Actuators. Advanced Electronic Materials, 2016, 2, 1500476.	2.6	37
78	Stress measurements of planar dielectric elastomer actuators. Review of Scientific Instruments, 2016, 87, 053901.	0.6	8
79	Tomographic brain imaging with nucleolar detail and automatic cell counting. Scientific Reports, 2016, 6, 32156.	1.6	57
80	Computational cell quantification in the human brain tissues based on hard x-ray phase-contrast tomograms. Proceedings of SPIE, 2016, , .	0.8	0
81	Tailoring the mass distribution and functional group density of dimethylsiloxane-based films by thermal evaporation. APL Materials, 2016, 4, .	2.2	8
82	Hierarchical imaging of the human knee. , 2016, , .		3
83	Comparing natural and artificial carious lesions in human crowns by means of conventional hard x-ray micro-tomography and two-dimensional x-ray scattering with synchrotron radiation. , 2016, , .		2
84	Electro-spraying and ultra-violet light curing of polydimethylsiloxane to fabricate thin films for low-voltage dielectric elastomer actuators. , 2016, , .		0
85	Morphology and conductivity of Au films on polydimethylsiloxane using (3-mercaptopropyl)trimethoxysilane (MPTMS) as an adhesion promoter. Proceedings of SPIE, 2016, , .	0.8	9
86	Comparing the accuracy of master models based on digital intra-oral scanners with conventional plaster casts. Physics in Medicine, 2016, 1, 20-26.	0.6	26
87	Middle ear bones of a mid-gestation ruminant foetus extracted from x-ray computed tomography. , 2016, , .		2
88	Histology-validated x-ray tomography for imaging human coronary arteries. Proceedings of SPIE, 2016,	0.8	0
89	The petrosal bone and bony labyrinth of early to middle Miocene European deer (Mammalia, Cervidae) reveal their phylogeny. Journal of Morphology, 2016, 277, 1329-1338.	0.6	22
90	Extending two-dimensional histology into the third dimension through conventional micro computed tomography. NeuroImage, 2016, 139, 26-36.	2.1	69

#	Article	IF	CITATIONS
91	Characterization of mechano-sensitive nano-containers for targeted vasodilation. Proceedings of SPIE, 2016, , .	0.8	2
92	X-ray micro-tomography for investigations of brain tissues on cellular level. , 2016, , .		3
93	Imaging tissues for biomedical research using the high-resolution micro-tomography system nanotomÂ $^{\odot}$ m. Proceedings of SPIE, 2016, , .	0.8	0
94	Hard x-ray micro-tomography of a human head post-mortem as a gold standard to compare x-ray modalities. , 2016, , .		1
95	Automatic histology registration in application to x-ray modalities. Proceedings of SPIE, 2016, , .	0.8	1
96	Non-destructive phase contrast hard x-ray imaging to reveal the three-dimensional microstructure of soft and hard tissues. , 2016, , .		2
97	Characterization of ultraviolet light cured polydimethylsiloxane films for low-voltage, dielectric elastomer actuators. , 2016, , .		1
98	Molecular beam deposition of high-permittivity polydimethylsiloxane for nanometer-thin elastomer films in dielectric actuators. Materials and Design, 2016, 105, 106-113.	3.3	12
99	Biomimetic artificial sphincter muscles: status and challenges. Proceedings of SPIE, 2016, , .	0.8	3
100	Thin Film Formation and Morphology of Electrosprayed Polydimethylsiloxane. Langmuir, 2016, 32, 3276-3283.	1.6	10
101	Artificial Muscle Devices: Innovations and Prospects for Fecal Incontinence Treatment. Annals of Biomedical Engineering, 2016, 44, 1355-1369.	1.3	47
102	Surprising lack of liposome-induced complement activation by artificial 1,3-diamidophospholipids in vitro. Nanomedicine: Nanotechnology, Biology, and Medicine, 2016, 12, 845-849.	1.7	18
103	Imaging the Human Body Down to the Molecular Level. , 2016, , 1-10.		Ο
104	Imaging the Human Body Down to the Molecular Level. , 2016, , 1501-1510.		0
105	High-resolution synchrotron radiation-based phase tomography of the healthy and epileptic brain. , 2016, , .		Ο
106	Micro- and nanostructured electro-active polymer actuators as smart muscles for incontinence treatment. AIP Conference Proceedings, 2015, , .	0.3	5
107	Midâ€regional proâ€atrial natriuretic peptide and the assessment of volaemic status and differential diagnosis of profound hyponatraemia. Journal of Internal Medicine, 2015, 278, 29-37.	2.7	11
108	Mineralization of Early Stage Carious Lesions In Vitro—A Quantitative Approach. Dentistry Journal, 2015, 3, 111-122.	0.9	19

#	Article	IF	CITATIONS
109	Ultraviolet–ozone surface cleaning of injectionâ€molded, thermoplastic microcantilevers. Journal of Applied Polymer Science, 2015, 132, .	1.3	3
110	Siloxane-based thin films for biomimetic low-voltage dielectric actuators. Sensors and Actuators A: Physical, 2015, 233, 32-41.	2.0	38
111	Strain-dependent characterization of electrode and polymer network of electrically activated polymer actuators. Proceedings of SPIE, 2015, , .	0.8	1
112	High-resolution x-ray computed tomography to understand ruminant phylogeny. Proceedings of SPIE, 2014, , .	0.8	2
113	Characterization of a human tooth with carious lesions using conventional and synchrotron radiation-based micro computed tomography. Proceedings of SPIE, 2014, , .	0.8	2
114	Grating interferometry-based phase microtomography of atherosclerotic human arteries. Proceedings of SPIE, 2014, , .	0.8	3
115	Three-dimensional imaging of human hippocampal tissue using synchrotron radiation- and grating-based micro computed tomography. Proceedings of SPIE, 2014, , .	0.8	1
116	Tumors in murine brains studied by grating-based phase contrast microtomography. , 2014, , .		0
117	Three-dimensional registration of synchrotron radiation-based micro-computed tomography images with advanced laboratory micro-computed tomography data from murine kidney casts. , 2014, , .		1
118	Assessing the grain structure of highly X-ray absorbing metallic alloys. International Journal of Materials Research, 2014, 105, 692-701.	0.1	2
119	Experimental comparison of grating- and propagation-based hard X-ray phase tomography of soft tissue. Journal of Applied Physics, 2014, 116, .	1.1	46
120	Impact of electrode preparation on the bending of asymmetric planar electro-active polymer microstructures. Proceedings of SPIE, 2014, , .	0.8	2
121	Position paper from the IBRA Symposium on Surgery of the Head – The 2nd International Symposium for Condylar Fracture Osteosynthesis, Marseille, France 2012. Journal of Cranio-Maxillo-Facial Surgery, 2014, 42, 1234-1249.	0.7	70
122	Combining micro computed tomography and three-dimensional registration to evaluate local strains in shape memory scaffolds. Acta Biomaterialia, 2014, 10, 1024-1034.	4.1	24
123	Differentiation of human mesenchymal stem cells on plasma-treated polyetheretherketone. Journal of Materials Science: Materials in Medicine, 2014, 25, 515-525.	1.7	77
124	Damping of Selective-Laser-Melted NiTi for Medical Implants. Journal of Materials Engineering and Performance, 2014, 23, 2614-2619.	1.2	27
125	Nanostructure of carious tooth enamel lesion. Acta Biomaterialia, 2014, 10, 355-364.	4.1	30
126	Complementary X-ray tomography techniques for histology-validated 3D imaging of soft and hard tissues using plaque-containing blood vessels as examples. Nature Protocols, 2014, 9, 1401-1415.	5.5	55

#	Article	IF	CITATIONS
127	Combined use of micro computed tomography and histology to evaluate the regenerative capacity of bone grafting materials. International Journal of Materials Research, 2014, 105, 679-691.	0.1	42
128	Microstructure of selective laser melted nickel–titanium. Materials Characterization, 2014, 94, 189-202.	1.9	176
129	Tailoring surface nanostructures on polyaryletherketones for load-bearing implants. European Journal of Nanomedicine, 2014, 6, .	0.6	6
130	Rapid prototyped porous nickel–titanium scaffolds as bone substitutes. Journal of Tissue Engineering, 2014, 5, 204173141454067.	2.3	33
131	Histology to μCT Data Matching Using Landmarks and a Density Biased RANSAC. Lecture Notes in Computer Science, 2014, 17, 243-250.	1.0	10
132	Mechanical and chemical stability of injectionâ€molded microcantilevers used for sensing. Journal of Applied Polymer Science, 2013, 127, 2363-2370.	1.3	7
133	The use of shear stress for targeted drug delivery. Cardiovascular Research, 2013, 99, 328-333.	1.8	72
134	Equipment automation framework with embedded Interface-A. , 2013, , .		0
135	Measuring the bending of asymmetric planar EAP structures. Proceedings of SPIE, 2013, , .	0.8	1
136	Holotomography versus X-ray grating interferometry: A comparative study. Applied Physics Letters, 2013, 103, .	1.5	36
137	Assessing the morphology of selective laser melted NiTi-scaffolds for a three-dimensional quantification of the one-way shape memory effect. , 2013, , .		12
138	Nanodentistry. Nanoscience and Technology, 2012, , 95-107.	1.5	4
139	Multimodal imaging of human cerebellum - merging X-ray phase microtomography, magnetic resonance microscopy and histology. Scientific Reports, 2012, 2, 826.	1.6	57
140	Evaluation of oral scanning in comparison to impression using three-dimensional registration. Proceedings of SPIE, 2012, , .	0.8	2
141	Anisotropy in polyetheretherketone films. Journal of Nanophotonics, 2012, 6, 063510.	0.4	1
142	Three-dimensional registration of tomography data for quantification in biomaterials science. International Journal of Materials Research, 2012, 103, 242-249.	0.1	32
143	Grating-based tomography of human tissues. AIP Conference Proceedings, 2012, , .	0.3	5
144	Nanometer-size anisotropy of injection-molded polymer micro-cantilever arrays. Journal of Applied Physics, 2012, 111, 103530.	1.1	1

#	Article	IF	CITATIONS
145	Comparison of propagation-based phase-contrast tomography approaches for the evaluation of dentin microstructure. Proceedings of SPIE, 2012, , .	0.8	4
146	Morphology of atherosclerotic coronary arteries. Proceedings of SPIE, 2012, , .	0.8	6
147	Comparison of denture models by means of micro computed tomography. , 2012, , .		6
148	Comparing the micro-vascular structure of cancerous and healthy tissues. Proceedings of SPIE, 2012, , .	0.8	4
149	Nanostructuring polyetheretherketone for medical implants. European Journal of Nanomedicine, 2012, 4, .	0.6	11
150	Designing micro- and nanostructures for artificial urinary sphincters. Proceedings of SPIE, 2012, , .	0.8	8
151	Shear Stress as Drug Delivery Trigger. Chimia, 2012, 66, 715.	0.3	1
152	Asymmetric rotational axis reconstruction of grating-based x-ray phase contrast tomography of the human cerebellum. Proceedings of SPIE, 2012, , .	0.8	4
153	Combined micro computed tomography and histology study of bone augmentation and distraction osteogenesis. , 2012, , .		4
154	Controlling Mechanical Properties of NiTi Scaffolds built by Selective Laser Melting. Biomedizinische Technik, 2012, 57, .	0.9	1
155	Automatic selection of a representative trial from multiple measurements using Principle Component Analysis. Journal of Biomechanics, 2012, 45, 2306-2309.	0.9	30
156	In Vivo Toxicity of Titanium Dioxide and Gold Nanoparticles. , 2012, , 1083-1090.		0
157	Three-dimensional quantification of capillary networks in healthy and cancerous tissues of two mice. Microvascular Research, 2012, 84, 314-322.	1.1	46
158	Tailoring Selective Laser Melting Process Parameters for NiTi Implants. Journal of Materials Engineering and Performance, 2012, 21, 2519-2524.	1.2	171
159	Micro- and nanostructured polymer substrates for biomedical applications. Proceedings of SPIE, 2012,	0.8	12
160	Insect Flight and Micro Air Vehicles (MAVs). , 2012, , 1096-1109.		0
161	Global and local hard X-ray tomography of a centimeter-size tumor vessel tree. Journal of Synchrotron Radiation, 2012, 19, 114-125.	1.0	4
162	Shear-stress sensitive lenticular vesicles for targeted drug delivery. Nature Nanotechnology, 2012, 7, 536-543.	15.6	248

#	Article	IF	CITATIONS
163	Cracks in dentin and enamel after cryopreservation. Oral Surgery, Oral Medicine, Oral Pathology and Oral Radiology, 2012, 113, e5-e10.	0.2	13
164	Understanding Nano-Anatomy of Healthy and Carious Human Teeth: a Prerequisite for Nanodentistry. Biointerphases, 2012, 7, 4.	0.6	30
165	Nano-Mechanical Transduction of Polymer Micro-Cantilevers to Detect Bio-Molecular Interactions. Biointerphases, 2012, 7, 6.	0.6	7
166	Imaging the Human Body: Micro- and Nanostructure of Human Tissues. Nanoscience and Technology, 2012, , 69-94.	1.5	3
167	Three-dimensional morphology and mechanics of bone scaffolds fabricated by rapid prototyping. International Journal of Materials Research, 2012, 103, 200-206.	0.1	6
168	Tilting the jaw to improve the image quality or to reduce the dose in cone-beam computed tomography. European Journal of Radiology, 2011, 80, e389-e393.	1.2	23
169	Impact of adhesive surface and volume of luting resin on fracture resistance of root filled teeth. International Endodontic Journal, 2011, 44, 432-439.	2.3	16
170	Nanostructure of healthy and caries-affected human teeth. Nanomedicine: Nanotechnology, Biology, and Medicine, 2011, 7, 694-701.	1.7	68
171	Three-dimensional strain fields in human brain resulting from formalin fixation. Journal of Neuroscience Methods, 2011, 202, 17-27.	1.3	62
172	Surface patterned polymer micro-cantilever arrays for sensing. Sensors and Actuators A: Physical, 2011, 172, 2-8.	2.0	33
173	X-ray Grating Interferometry at ESRF: Applications and Recent Technical Developments. , 2011, , .		1
174	Realâ€ŧime measurements of human chondrocyte heat production during in vitro proliferation. Biotechnology and Bioengineering, 2011, 108, 3019-3024.	1.7	7
175	Contractile cell forces exerted on rigid substrates. , 2011, 21, 479-487.		14
176	Evaluating the microstructure of human brain tissues using synchrotron radiation-based micro-computed tomography. Proceedings of SPIE, 2010, , .	0.8	10
177	Recent developments in x-ray Talbot interferometry at ESRF-ID19. Proceedings of SPIE, 2010, , .	0.8	32
178	X-ray grating interferometer for imaging at a second-generation synchrotron radiation source. Proceedings of SPIE, 2010, , .	0.8	6
179	Disposable polymeric micro-cantilever arrays for sensing. Procedia Engineering, 2010, 5, 347-350.	1.2	9
180	Tailoring biocompatibility: Benefitting patients. Materials Today, 2010, 13, 58.	8.3	15

#	Article	IF	CITATIONS
181	Nanomethods: Scanning X-ray scattering: Evaluating the nanostructure of human tissues. European Journal of Nanomedicine, 2010, 3, .	0.6	20
182	Evaluating tooth restorations: micro-computed tomography in practical training for students in dentistry. , 2010, , .		4
183	The morphology of amputated human teeth and its relation to mechanical properties after restoration treatment. , 2010, , .		3
184	Morphology of urethral tissues. Proceedings of SPIE, 2010, , .	0.8	10
185	The microstructure of mandibular bone grafts and three-dimensional cell clusters. , 2010, , .		1
186	Computed tomography to quantify tooth abrasion. Proceedings of SPIE, 2010, , .	0.8	3
187	Determination of strain fields in porous shape memory alloys using micro-computed tomography. Proceedings of SPIE, 2010, , .	0.8	11
188	Mikro-Computertomographie für die dreidimensionale Charakterisierung von Implantaten und Geweben. Sports Orthopaedics and Traumatology, 2010, 26, 145-151.	0.1	1
189	High-resolution tomographic imaging of a human cerebellum: comparison of absorption and grating-based phase contrast. Journal of the Royal Society Interface, 2010, 7, 1665-1676.	1.5	149
190	Bio-inspired dental fillings. Proceedings of SPIE, 2009, , .	0.8	10
191	Bio-mimetic hollow scaffolds for long bone replacement. Proceedings of SPIE, 2009, , .	0.8	6
192	Highâ€resolution Xâ€ray tomography of the human inner ear: synchrotron radiationâ€based study of nerve fibre bundles, membranes and ganglion cells. Journal of Microscopy, 2009, 234, 95-102.	0.8	78
193	Systemic allergic dermatitis reaction to nickel released from an eyelet in an intravenous catheter. Contact Dermatitis, 2009, 61, 180-182.	0.8	10
194	The cochlea in fetuses with neural tube defects. International Journal of Developmental Neuroscience, 2009, 27, 669-676.	0.7	7
195	Pelizaeus Merzbacher disease: morphological analysis of the vestibulo-cochlear system. Acta Oto-Laryngologica, 2009, 129, 1395-1399.	0.3	7
196	High-sensitivity phase-contrast tomography of rat brain in phosphate buffered saline. Journal of Physics: Conference Series, 2009, 186, 012046.	0.3	13
197	Visualization of tumor vessels using synchrotron radiation-based micro computed tomography. Journal of Physics: Conference Series, 2009, 186, 012088.	0.3	1
198	Strain fields in histological slices of brain tissue determined by synchrotron radiation-based micro computed tomography. Journal of Neuroscience Methods, 2008, 170, 149-155.	1.3	28

#	Article	IF	CITATIONS
199	The morphology of anisotropic 3D-printed hydroxyapatite scaffolds. Biomaterials, 2008, 29, 3799-3806.	5.7	190
200	High density resolution in synchrotron-radiation-based attenuation-contrast microtomography. Proceedings of SPIE, 2008, , .	0.8	53
201	Angiofil: a novel radio-contrast agent for post-mortem micro-angiography. Proceedings of SPIE, 2008, , ·	0.8	2
202	Internal structures of scaffold-free 3D cell cultures visualized by synchrotron radiation-based micro-computed tomography. , 2008, , .		3
203	Synchrotron radiation-based micro computed tomography in the assessment of dentin de- and re-mineralization. , 2008, , .		3
204	High-resolution tomographic imaging of microvessels. Proceedings of SPIE, 2008, , .	0.8	42
205	Quality assessment of clinical computed tomography. Proceedings of SPIE, 2008, , .	0.8	4
206	Comparative study of desktop- and synchrotron radiation-based micro computed tomography analyzing cell-seeded scaffolds in tissue engineering of bone. , 2008, , .		4
207	Comparative micro computed tomography study of a vertebral body. Proceedings of SPIE, 2008, , .	0.8	10
208	Comparison between x-ray tube-based and synchrotron radiation-based μCT. Proceedings of SPIE, 2008, ,	0.8	46
209	Simulation of stress urinary incontinence for in-vitro studies. Technology and Health Care, 2008, 16, 77-83.	0.5	2
210	Morphology of bony tissues and implants uncovered by high-resolution tomographic imaging. International Journal of Materials Research, 2007, 98, 613-621.	0.1	44
211	Minipig urethra: A suitable animal model in vitro. Technology and Health Care, 2007, 20, 329-336.	0.5	5
212	Circulating levels of copeptin, a novel biomarker, in lower respiratory tract infections. European Journal of Clinical Investigation, 2007, 37, 145-152.	1.7	179
213	Image Based Analysis of Bone Graft Samples made by 3D Printing Using Conventional and Synchrotron-Radiation-Based Micro-Computed Tomography. , 2007, , 121-126.		3
214	Bone marrow derived mesenchymal stem cells isolated from patients with diabetes mellitus type 1 are able to induce a pancreatic endocrine genes in vitro. Journal of Stem Cells and Regenerative Medicine, 2007, 2, 102-3.	2.2	1
215	3D analysis of bone formation around titanium implants using micro computed tomography (l̂¼CT). , 2006, , .		4
216	Three-Dimensional Characterization of Cell Clusters Using Synchrotron-Radiation-Based Micro-Computed Tomography. Microscopy and Microanalysis, 2006, 12, 97-105.	0.2	24

#	Article	IF	CITATIONS
217	Circulating levels of pro-atrial natriuretic peptide in lower respiratory tract infections. Journal of Internal Medicine, 2006, 260, 568-576.	2.7	58
218	Blood vessel staining in the myocardium for 3D visualization down to the smallest capillaries. Nuclear Instruments & Methods in Physics Research B, 2006, 246, 254-261.	0.6	22
219	Three-dimensional assessment of brain tissue morphology. , 2006, 6318, 9.		5
220	Optimization of the artificial urinary sphincter: modelling and experimental validation. Physics in Medicine and Biology, 2006, 51, 1361-1375.	1.6	19
221	Anatomy of the murine and human cochlea visualized at the cellular level by synchrotron-radiation-based micro-computed tomography. , 2006, , .		6
222	Visualising complex morphology of fatigue cracks in voxel based 3D datasets. Materials Science and Technology, 2006, 22, 1038-1044.	0.8	9
223	Image-based analysis of the internal microstructure of bone replacement scaffolds fabricated by 3D printing. , 2006, 6318, 64.		2
224	Tomography studies of biological cells on polymer scaffolds. Journal of Physics Condensed Matter, 2004, 16, S3499-S3510.	0.7	10
225	An optimization procedure for spatial and density resolution in hard X-ray micro-computed tomography. Nuclear Instruments & Methods in Physics Research B, 2004, 225, 599-603.	0.6	62
226	Functional micro-imaging of soft and hard tissue using synchrotron light. , 2004, , .		4
227	Comparison of Microfocus- and Synchrotron X-ray Tomography for the Analysis of Osteointegration around Ti6Al4V Implants. , 2004, 7, 42-51.		101
228	Tomography studies of human foreskin fibroblasts on polymer yarns. Nuclear Instruments & Methods in Physics Research B, 2003, 200, 397-405.	0.6	24
229	Wood-Derived Porous Ceramics via Infiltration of SiO2-Sol and Carbothermal Reduction. Holzforschung, 2003, 57, 440-446.	0.9	20
230	Nondestructive three-dimensional evaluation of biocompatible materials by microtomography using synchrotron radiation. , 2002, , .		31
231	Resorbable defect analog PLGA scaffolds using CO2as solvent: Structural characterization. Journal of Biomedical Materials Research Part B, 2002, 62, 89-98.	3.0	65
232	Non-destructive three-dimensional evaluation of a polymer sponge by micro-tomography using synchrotron radiation. New Biotechnology, 2002, 19, 73-78.	2.7	73
233	Haemostatic profile in hypothyroidism as potential risk factor for vascular or thrombotic disease. European Journal of Clinical Investigation, 2001, 31, 131-137.	1.7	119
234	Protein adsorption and monocyte activation on germanium nanopyramids. Biomaterials, 2001, 22, 2307-2316.	5.7	80

#	Article	IF	CITATIONS
235	The stiffness of bone marrow cell–knit composites is increased during mechanical load. Biomaterials, 2001, 22, 3169-3178.	5.7	22
236	Impact of nanometer-scale roughness on contact-angle hysteresis and globulin adsorption. Journal of Vacuum Science & Technology an Official Journal of the American Vacuum Society B, Microelectronics Processing and Phenomena, 2001, 19, 1715.	1.6	90
237	NATURAL FORMATION OF NANOSTRUCTURES: FROM FUNDAMENTALS IN METAL HETEROEPITAXY TO APPLICATIONS IN OPTICS AND BIOMATERIALS SCIENCE. Surface Review and Letters, 2001, 08, 169-228.	0.5	31
238	Molecular beam epitaxy ofp-hexaphenyl on GaAs(111). Surface and Interface Analysis, 2000, 30, 518-521.	0.8	12
239	Degradation Kinetics of Biodegradable Fiber Composites. Journal of Polymers and the Environment, 2000, 8, 91-96.	2.4	8
240	Amino acid neurotransmitter metabolism in neurones and glia following kainate injection in rats. Neuroscience Letters, 2000, 279, 169-172.	1.0	20
241	Reduction of the bacterial load by the silver-coated endotracheal tube (SCET), a laboratory investigation. Technology and Health Care, 1999, 7, 359-370.	0.5	38
242	Dimer Pairing on the C-Alloyed Si(001) Surface. Physical Review Letters, 1999, 82, 972-975.	2.9	73
243	In-plane alignment of noncentrosymmetric molecules by oblique-incidence molecular beam deposition. Applied Physics Letters, 1999, 74, 3110-3112.	1.5	10
244	Film thickness measurement and linear dichroism of organic thin films prepared by molecular beam deposition at oblique incidence. Optical Materials, 1999, 12, 345-350.	1.7	7
245	Ordering of PVBA on amorphous SiO2 and Pd(110). Thin Solid Films, 1999, 343-344, 171-174.	0.8	5
246	Oblique Incidence Organic Molecular Beam Deposition and Nonlinear Optical Properties of Organic Thin Films with a Stable In-Plane Directional Order. Advanced Materials, 1999, 11, 745-749.	11.1	34
247	In situ scanning tunneling microscopy study of C-induced Ge quantum dot formation on Si(100). Applied Physics Letters, 1999, 74, 994-996.	1.5	42
248	Binding and ordering of large organic molecules on an anisotropic metal surface: PVBA on Pd(110). Surface Science, 1999, 431, 168-173.	0.8	26
249	Epitaxial growth of para-hexaphenyl on GaAs(001)-2×4. Surface Science, 1999, 437, 191-197.	0.8	21
250	A UHV STM for in situ characterization of MBE/CVD growth on 4-inch wafers. Applied Physics A: Materials Science and Processing, 1998, 66, S993-S997.	1.1	14
251	MBE growth of para-hexaphenyl on GaAs(001)-2×4. Surface Science, 1998, 418, 256-266.	0.8	43
252	Self-Assembly in Ultrahigh Vacuum:Â Growth of Organic Thin Films with a StableIn-PlaneDirectional Order. Journal of the American Chemical Society, 1998, 120, 8563-8564.	6.6	44

#	Article	IF	CITATIONS
253	Strain Relief via Island Ramification in Submonolayer Hereroepitaxy. Surface Review and Letters, 1998, 05, 769-781.	0.5	18
254	Island Shape Transition in Heteroepitaxial Metal Growth on Square Lattices. Physical Review Letters, 1998, 80, 2642-2645.	2.9	50
255	Ge-Quantum Dots on SI(001) Tailored by Carbon Predeposition. Materials Research Society Symposia Proceedings, 1998, 533, 183.	0.1	8
256	Inelastic Scattering in Reflection High-Energy Electron Diffraction from Si(111). Physical Review Letters, 1997, 79, 4393-4396.	2.9	3
257	NUCLEATION AND GROWTH OF Cu/Ni(100): A VARIABLE TEMPERATURE STM STUDY. Surface Review and Letters, 1997, 04, 1161-1165.	0.5	5
258	A comparative STM and SPA-LEED study on the evolution of strain induced stripe pattern on Cu/Ni(100). Surface Science, 1997, 376, 113-122.	0.8	13
259	Comparison of reflection high-energy electron diffraction and low-energy electron diffraction using high-resolution instrumentation. Surface Science, 1997, 389, 338-348.	0.8	11
260	Submonolayer Nucleation and Growth of Copper on Ni(100). NATO ASI Series Series B: Physics, 1997, , 151-159.	0.2	2
261	Initial stages of Cu epitaxy on Ni(100): Postnucleation and a well-defined transition in critical island size. Physical Review B, 1996, 54, 17858-17865.	1.1	84
262	Strain relief in metal heteroepitaxy on faceâ€centeredâ€cubic(100): Cu/Ni(100). Journal of Vacuum Science and Technology A: Vacuum, Surfaces and Films, 1996, 14, 1878-1881.	0.9	20
263	Strain Relief at Metal Interfaces with Square Symmetry. Physical Review Letters, 1996, 76, 2358-2361.	2.9	58
264	SPAâ€RHEED—A novel method in reflection highâ€energy electron diffraction with extremely high angular and energy resolution. Review of Scientific Instruments, 1995, 66, 5232-5235.	0.6	20
265	Impaired Action of Thyroid Hormone Associated with Smoking in Women with Hypothyroidism. New England Journal of Medicine, 1995, 333, 964-969.	13.9	149
266	Strain-induced dimer adatom stacking fault structures of germanium on Si(111)-(â^š3×â^š3)R30º:B observed by scanning tunneling microscopy. Journal of Vacuum Science & Technology an Official Journal of the American Vacuum Society B, Microelectronics Processing and Phenomena, 1992, 10, 16.	1.6	7
267	Trench formation in surfactant mediated epitaxial film growth of Ge on Si(100). Applied Physics A: Solids and Surfaces, 1992, 54, 265-269.	1.4	11
268	Layer-by-layer growth of germanium on Si(100): strain-induced morphology and the influence of surfactants. Ultramicroscopy, 1992, 42-44, 832-837.	0.8	111
269	Strained-layer growth and islanding of germanium on Si(111)-(7 × 7) studied with STM. Surface Science, 1991, 248, 321-331.	0.8	177
270	On the thermal behaviour of molecular beam effusion sources. Crystal Research and Technology, 1990, 25, 1087-1095.	0.6	2

#	Article	IF	CITATIONS
271	Phase-contrast x-ray tomography reveals the micro-anatomy of soft tissues. SPIE Newsroom, 0, , .	0.1	1
272	Imaging the orientation of myelin sheaths in a non-stained histology slide of human brain. Precision Nanomedicine, 0, , .	0.4	2